IEEE Access
Multidisciplinary | Rapid Review | Open Access Journal

Received November 25, 2019, accepted December 14, 2019, date of publication December 26, 2019,
date of current version January 9, 2020.

Digital Object Identifier 10.1109/ACCESS.2019.2962381

Numerical Studies of Electrokinetically Controlled Concentration of Diluted DNA Molecules in a T-Shaped Microchannel

YANLI GONG, HAI JIANG, YUNFEI BAI, ZIJIAN WU, BEI PENG, AND XUAN WENG
School of Mechanical and Electrical Engineering, University of Electronic Science and Technology of China, Chengdu 611731, China

Corresponding author: Xuan Weng (xuanweng@uestc.edu.cn)

This work was supported in part by the National Natural Science Foundation of China under Grant 31771078, and in part by the Fundamental Research Funds for the Central Universities under Grant ZYGX2019J036.

ABSTRACT Sample concentration is extremely important in microfluidic detection systems, especially for the detection of trace substance. Among various sample concentration techniques used in microfluidic devices, direct electrokinetic trapping is more convenient and easier to realize. In this paper, a T-shaped microchannel configuration was developed to achieve electrokinetic concentration. Numerical simulation analysis on two-dimensional (2D) configuration model were performed. The microfluidic configuration for DNA enrichment was firstly optimized by analyzing various field distributions. Then, the influence of selected dimension and electrical parameters on enrichment rate was analyzed, including size of the transition chamber and enrichment chamber, distance between the inlet branches, length of the inlet vertical branches, size of the electrode and the electric field intensity. With optimized parameters, our model is able to achieve an optimal enrichment rate of 234.2 at an applied voltage of 20 V within a period of 1200s. Our method provides a valuable guidance for the design of an easy-controlled microfluidic system of precise enrichment capability.

INDEX TERMS Sample concentration, electrokinetic concentration, electroosmotic flow, electroosmotic induced pressure flow, enrichment.

I. INTRODUCTION

Microfluidics has been increasingly used in various detection systems since its development in the 1980s, including disease diagnosis [1]–[3], drug analysis [4], [5], food safety [6], [7], environment monitoring [8], [9], and many others [10]–[12]. Microfluidic technology has many advantages over traditional detection methods such as simple operation, low cost, small volume and small reagent consumption. In a microfluidic device, the amount of the substance to be tested directly affects the detection accuracy and sensitivity, especially in the detection of dilute substances. For example, the recently reported presence of microplastics and nanoplastics in human body, the presence of certain allergens in food, the very small amount of tumor cells in the early stage of cancer, all require urgent sample pretreatment to reach the detection limit of target components. Sample concentration is one of the common and important pretreatment methods, which aims to realize the accurate detection of trace substances. Some of sample concentration methods in microfluidic devices had been summarized in previous literatures [13]–[15]. Those methods can be classified into the following categories. Stacking method, including sweeping [16]–[19], field amplified sample stacking (FASS) [20]–[23] and isotachophoresis (ITP) [24]–[27], is based on a sudden change of the electrophoretic velocity of analyte caused by different electric field intensity. Focusing method is on the basis of field gradient equilibrium and accomplished by creating corresponding gradient field, such as isoelectric focusing (IEF) [28]–[30], electric field gradient focusing (EFGF) [31]–[33], temperature gradient focusing (TGF) [34]–[37] and ion concentration polarization focusing (ICP) [38]–[41]. In addition to above mentioned methods, some other trapping mechanisms are also reported including dielectrophoretic trapping (DEPT) [42]–[44], immunocapture-based trapping (ICBT) [45], [46], magnetic beads assisted concentration [47] and static concentration

The associate editor coordinating the review of this manuscript and approving it for publication was Karol Malecha.

methods based on special configurations [48] or filtering membranes [49].

Microfluidic concentration based on electric field effect has been developed rapidly in recent years as the electric field theory was fully developed and it is easy to be integrated into the microfluidic chip. As mentioned above, ICP which utilizes the ion selective membranes or microchannel-nanochannel junctions for concentrating has drawn wide attention due to its high enrichment efficiency. To date, however, the research of this area has mainly focused on the elaboration of the mechanism and the exploration of the factors influencing the efficiency of ion enrichment by numerical studies. For example, Jia and Kim [50] established a 2-D model and performed a numerical analysis on the ICP phenomena, in which they revealed the factors that affected the concentration enrichment rate and provided good guidelines to make use of ICP to achieve more effective preconcentration. Similarly, Gong *et al.* [51] also carried out a 2D numerical analysis for Li+ preconcentration from high Mg2+/Li+ ratio brines based on ICP. The results presented the effect of the external pressure and cross-membrane voltages on the properties of Li+ through nanometer membrane. Although this method made some progress in practical applications, the limited flux velocity and complex fabrication of the nanometer across-chamber become the bottleneck for its further development.

Comparatively, direct electrokinetic trapping is more convenient and easier to be applied in microfluidic devices. The research group of Dongqing Li studied the mechanism of direct electrokinetics using voltage-bearing electrodes to enrich trace substances in sample solution [52], [53]. In 2010, Daghighi and Li [52] made a numerical study of electrokinetic concentration of DNA molecules in a closed-end microchannel. They analyzed the influencing factors of the electrokinetic-concentration process in a straight channel, including the channel dimensions, electrode size, applied electric field and so on. Later, Jiang *et al.* [53] experimentally validated the model in a microfluidic device to concentrate DNA molecules. The experimental results highly agreed with the numerical simulation, which well verified the effectiveness of this enrichment method. However, in the above enrichment systems, the enrichment and fluid driving modules were two independent parts, hence two separate sets of incentives were required. With the increasing demand of point-of-care testing, portable devices are expected to achieve the most comprehensive functions with the simplest configuration. In our previous study [54], we found an interesting phenomenon of particles blocking under an electroosmotic induced pressure-driven flow in a T-shaped microchannel. In this study, we expected to explore the mechanism behind this blocking phenomenon and put it into the practice of sample enrichment, so as to realize both functions of the sample solution driving and the substance concentration within a simple microfluidic chip. Based on our previous study, a novel theoretical model of the electrokinetically driven concentration process in a T-shaped microfluidic channel was developed. Numerical simulation was conducted by using software COMSOL. The flow field and coupled time-dependent concentration field in such microchannel were numerically studied. In this system, the combined effects of the electrokinetically-induced pressure-driven flow and the electrostatic force determine the final concentration field of the sample molecules. The influences of a number of parameters such as chamber dimensions, electrode size and the applied electric field were investigated in this study.

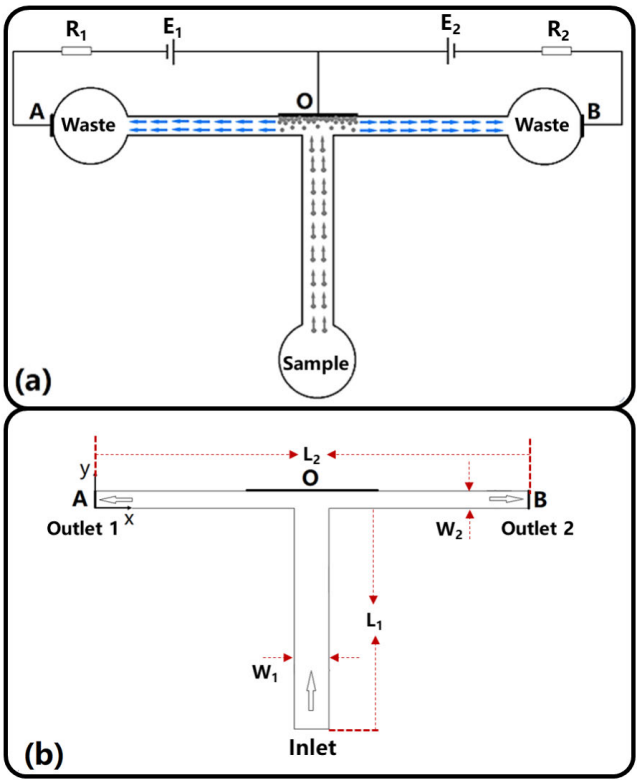

FIGURE 1. (a) Schematic diagram of driving and concentrating mechanism in a T-shaped microfluidic chip. (b) Simulation model of the T-shaped microfluidic chip.

II. PRINCIPLE AND SIMULATION MODEL

Fig. 1 (a) schematically illustrates the driving and concentrating mechanism of the developed microfluidic chip. The network consists of a sample reservoir, two waste reservoirs and a T-shaped channel. Three electrodes are placed at the waste reservoirs (electrode A and B) and middle of the horizontal microchannel (electrode O) to provide electric fields, respectively. Initially, three reservoirs are filled with buffer electrolytes at the same level. Voltages are then applied as shown Fig. 1 (a), to generate two streams of electroosmotic flow (EOF) from electrode O to electrode A and B, resulting in a strong negative pressure near the electrode O. Consequently, the solution in the sample reservoir will be inhaled towards the electrode O, and then flow into the waste reservoirs by EOFs. If charged substances present in the sample solution and the valence charge of which is opposite

to the polarity of electrode O, they will be accumulated in a certain range near electrode O due to the greater electrostatic force between the charged substances and electrode O compared with the electroosmotic drag force. In the previous studies [54] , we have successfully validated the feasibility of a microfluidic network to achieve electroosmotic induced pressure flow and accidentally found the blocking of particles at electrode O. In this study, we aimed to investigate the DNA molecules enrichment capability on the electrokinetically controlled T-shaped microfluidic chip by skillfully using the blocking phenomenon. According to the above principle, a numerical model (left-right symmetric) as shown in Fig. 1 (b) was established. L_1, L_2, W_1 and W_2 are the length and width of the vertical inlet channel and the horizontal outlet channel, respectively. It is worth noting that, in the model analysis, all the reservoirs were ignored to simplify the calculation as their dimensions are much larger than those of the channels thus the influence on the fluid is little.

In the preliminary simulation, it was found that the enrichment effect generated by the configuration in Fig. 1 was not sufficient. This is because that the enrichment area near the electrode O is an open area. Thus, although the charged substances can be accumulated near the electrode O due to the negative pressure and the electrostatic force, they would be still easy to be carried away by the drag force of the electroosmosis. Consequently, only the charged substances closed to the electrode O can be concentrated. To improve the enrichment efficiency, we established a novel configuration as shown in Fig. 2 (a) and (b). Compared to that in Fig. 1, the enrichment chamber and the transition chamber are added in both Fig. 2 (a) and (b) to trap the charged substances. In the enrichment chamber, strong negative pressure will suck the solution from the sample reservoir continuously. The charged substances flow into the enrichment chamber with the solution stream and then gather near the electrode O. Obviously, there are three streams flowing in the transition chamber. The main stream is the pressure-driven flow caused by the pressure difference between the inlet and the electrode O, occupying the middle part of transition chamber. Two side streams are the electroosmotic flows along the walls of the transition chamber generated by the electric fields. The direction of the side streams are opposite to that of the main stream. Some of the charged substances will flow out of the enrichment chamber with the side streams, however, the main stream may prevent the outflow of the charged substances like a 'gate'. Consequently, more and more charged substances will be trapped in the enrichment chamber. Over time, the inflow and outflow of the charged substances will reach an equilibrium. In order to further improve the enrichment effect, we established another configuration as shown in Fig. 2 (c) and (d). Compared with Fig. 2 (a) and (b), it has two more branch channels. The length and width of the vertical and horizontal channels are also symbolled with L_1, L_2, W_1 and W_2, respectively. While the length and the width of the transition chamber and enrichment chamber are labeled with L_3, L_4, W_3 and W_4, respectively. The length and the

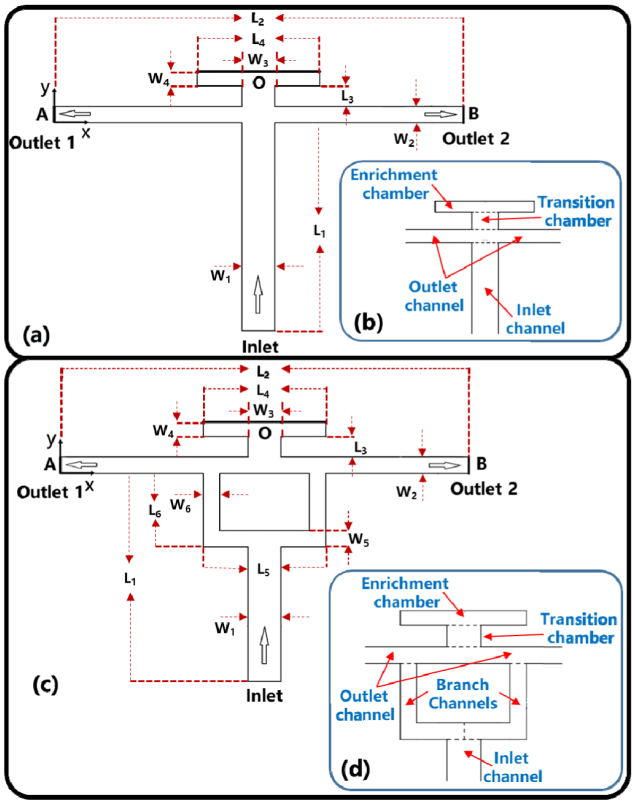

FIGURE 2. Schematic and channel partition diagram of the two improved configuration. (a) and (b) The configuration with the transition chamber and enrichment chamber. (c) and (d) The configuration with the transition chamber, enrichment chamber and two branch channels.

width of the horizontal and vertical branches are labelled with L_5, W_5, L_6 and W_6, respectively. The added branch channels can also generate the convective flow in the horizontal channel to form the second 'gate' to prevent the outflow of the charged substances. In this study, the change of velocity in z-direction is very small [55] and thus the two-dimensional (2D) model is sufficient to obtain a qualitative analysis of the influence of various parameters on the enrichment effect, we only considered the 2D model to perform the numerical analysis.

III. GOVERNING EQUATIONS AND NUMERICAL METHOD

A. GOVERNING EQUATIONS

Three governing equations are applied in the simulation models. Poisson equation is used to describe the electric field applied to the channel. Navier-Stokes equation is used to describe the incompressible laminar flow. And Nernst-Planck equation is used to describe the ions and molecules transport.

The static electric field can be interpreted in terms of Poisson equation as follows:

$$-\nabla \cdot (\sigma \nabla V - J_e) = 0 \tag{1}$$

where σ is the electrical conductivity, V is the electric potential, Je is an externally generated current density. All the walls of the microchannel are insulated. And V_{OA} has the same value as V_{OB}.

The flow field can be presented by the continuity equation and the vector equation as follows. They represent the conservation of mass and conservation of momentum respectively.

$$\rho(u \cdot \nabla)u = \nabla \cdot [-pI + \mu(\nabla u + (\nabla u)^T)] + F \quad (2)$$

$$\rho \nabla \cdot (u) = 0 \quad (3)$$

$$S = {}^1\!/_2(\nabla u + (\nabla u)^T) \quad (4)$$

where ρ is the density of the fluid, u is the velocity vector, p is pressure, I is the unit vector, μ is the dynamic viscosity, F is the volume force vector (can be ignored in this model), S is the strain-rate tensor. The velocity u can be used to illustrate the electroosmotic effect and obtained by following equations:

$$u = \mu_{eo} E \quad (5)$$

$$\mu_{eo} = -\frac{\varepsilon_r \varepsilon_0 \zeta}{\mu} \quad (6)$$

$$E = -\nabla V \quad (7)$$

where ε_0 is the permittivity of vacuum, ε_r is the relative permittivity of the fluid, ζ is the zeta potential, μ is the dynamic viscosity coefficient of the fluid.

The ionic species transport can be described by the following mass balance equations:

$$\nabla(-D_i \nabla c_i - z_i u_{m,i} F c_i \nabla V) + u \cdot \nabla c_i = R_i \quad (8)$$

$$u_{m,i} = D_i / R_i T \quad (9)$$

where D_i is the diffusion coefficient of species, c_i is the concentration of species, z_i is the charge number of species, $u_{m,i}$ is the mobility of species, F is the Faraday's constant, u denotes the fluid net velocity, R_i is the molar gas constant and T is the temperature. The sample solution flows into the T-shaped channel from the bottom, and an initial concentration of charged ions in the solution is given to solve the equation.

TABLE 1. Basic parameters used in the numerical simulation analysis.

	Attribute definition	Variable	Value	Unit
Fluid	conductivity	σ	0.11845	S/m
	Relative permittivity	ε	80.2	1
	Dynamic viscosity	μ	1×10-3	Pa.s
	density	ρ	1×103	kg/m3
DNA Molecules	Diffusion coefficient	D	1×10-10	m2/s
	Charge number	z	-1	1
	Initial concentration	c0	1.52×10-7	mol/m3
Others	Zeta potential	ζ	-40	mV
	temperature	T	293.15	K

B. NUMERICAL ANALYSIS

The numerical analysis was conducted by the software COMSOL 5.4. The 2D model is shown in Fig. 2. In order to ensure the accuracy of the computation, quadratic elements were used to discretize the solution domain. The basic parameters used in the simulation are summarized in Table 1.

IV. RESULTS AND DISCUSSION

For many biomedical applications, pre-concentration of sample molecules in a dilute solution is crucial, such as pre-concentration of viruses or DNA molecules. To obtain high efficiency of reaction or low limit of detection, concentration of sample molecules on a microfluidic device is critical. Therefore, our study aims to develop a method to concentrate DNA molecules in a dilute sample solution. In all simulations, the length (L_1) and width (W_1) of the inlet channel were fixed at 4 mm and 50 μm, respectively. While the length (L_2) and width (W_2) of the outlet channel were fixed at 8 mm and 25 μm, respectively. In Fig. 2 (c), the width of the horizontal (W_5) and vertical (W_6) branches were fixed at 25 μm, respectively. We defined them as invariants in all the simulations. The free solution mobility of DNA in a commonly used buffer, DI water, was used here. As presented in Table 1, single-standard DNA is chosen. The diffusion coefficient of DNA molecules is 1×10^{-10} m^2/s. The initial concentration in Inlet at t = 0 s was set to 1.52×10^{-7} mol/m^3.

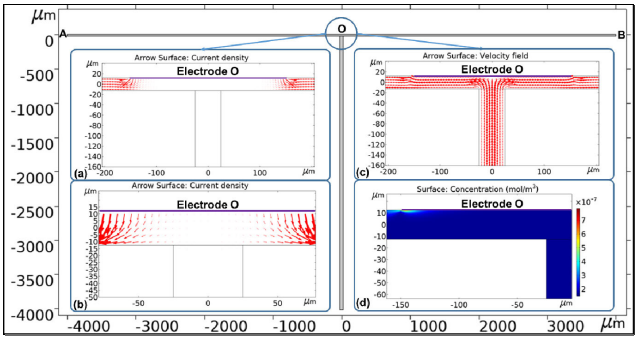

FIGURE 3. Simulation results of initial T-shaped configuration without any auxiliary channels. (a) and (b) The distribution of current density. (c) The distribution of flow velocity. (d) The distribution of concentration field. In this case, the voltages at electrode O, A and B were set to 0 V, 40V and 40V, respectively.

A. THE CONCENTRATION EFFECTS OF MICROFLUIDIC CHIP CONFIGURATIONS

In Fig. 1, when voltages at electrode O, A and B (as shown in bold purple line) were set to 0 V, 40V and 40V, respectively, the T-shaped microchannel without any auxiliary chambers presented very limited enrichment effect as shown in Fig. 3. It can be seen that the current density in Fig. 3 (a) and (b) gradually increases from the central area of the electrode O to both ends, and then becomes uniform towards the outlet channel. As seen from the velocity field in Fig. 3 (c), the fluid flows out of the inlet reservoir and evenly discharges to both ends of the microchannel A-B. Fig. 3 (d) illustrates the steady-state concentration field in the microchannel for the concentrating process. It is observed that two strong "adsorption areas" forming at both ends of the electrode O due to non-uniform electric field, and then uniformly distributes along the microchannel to the outlet. The reason for this is that the concentrated DNA molecules are carried away by the drag force of the electroosmosis. The simulation results show

that this configuration is not an ideal model for concentrating DNA molecules because the drag force of the electroosmosis is much greater than the electrostatic attraction force in most areas closed to the electrode O.

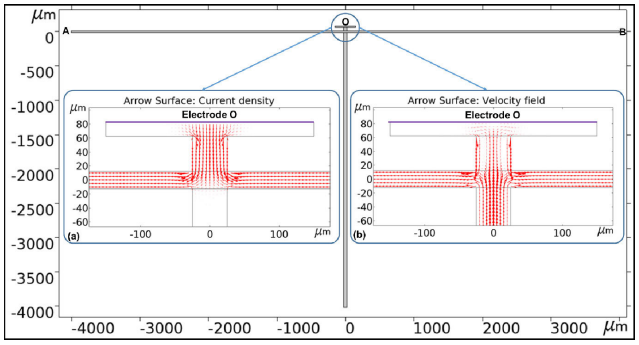

FIGURE 4. Simulation results of the improved configuration without the branch microchannels. (a) The distribution of current density. (b) The distribution of flow velocity. In this case, the voltages at electrode O, A and B are set to 0 V, 40V and 40V, respectively. The length (L_3) and width (W_3) of the transition chamber are 50 μm and 50 μm, respectively. The length (L_4) and width (W_4) of the enrichment chamber are 300 μm and 20 μm, respectively.

If the drag force of electroosmosis on the DNA molecules can be reduced as much as possible, the electrostatic attraction force will become dominated. The DNA molecules can be easily accumulated near the electrode O, resulting in dramatically increase enrichment rate. Based on this hypothesis, two improved configurations were designed as shown in Fig. 2. Fig. 4 represents the distributions of the current density and the flow field in the microchannels, respectively. As we mentioned above, three streams flow in the transition chamber. On one hand, the main stream caused by the pressure difference occupies the large area of the transition chamber, which continuously carries a large number of DNA molecules into the enrichment chamber and prevents the DNA molecules from escaping the enrichment chamber. On the other hand, the velocity of the flow decreases greatly in the enrichment chamber, which contributes to the concentration of the DNA molecules. The current density and the flow field analysis of the configuration in Fig. 2 (c) are shown in Fig. 5. As seen in Fig. 5 (a) and (b), the branch channels can generate convective flow in the horizontal channel. Similar to the streams in the transition chamber, the convective flow takes a step further in blocking the outflow of DNA molecules.

In this case, the voltages at electrode O, A and B were set to 0 V, 40V and 40V, respectively. The length (L_3) and width (W_3) of the transition chamber are 50 μm and 50 μm, respectively. The length (L_4) and width (W_4) of the enrichment chamber are 300 μm and 20 μm, respectively. The length of the horizontal (L_5) and vertical (L_6) branches are 300 μm and 200 μm, respectively.

Fig. 6 (a) and (b) present the concentration process as a function of time for the two improved configurations. At t = 0 s, the blue color indicates that the solution has no

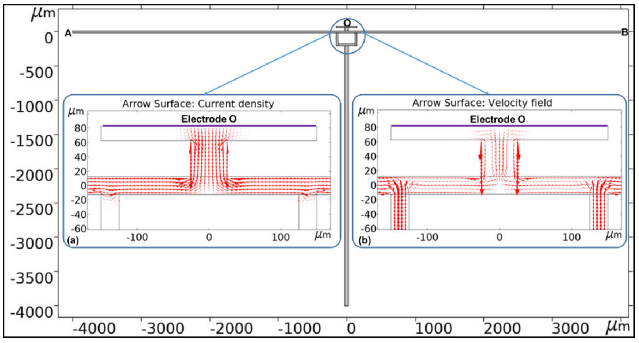

FIGURE 5. Improved configuration with branch microchannels. (a) The distribution of current density. (b) The distribution of flow velocity.

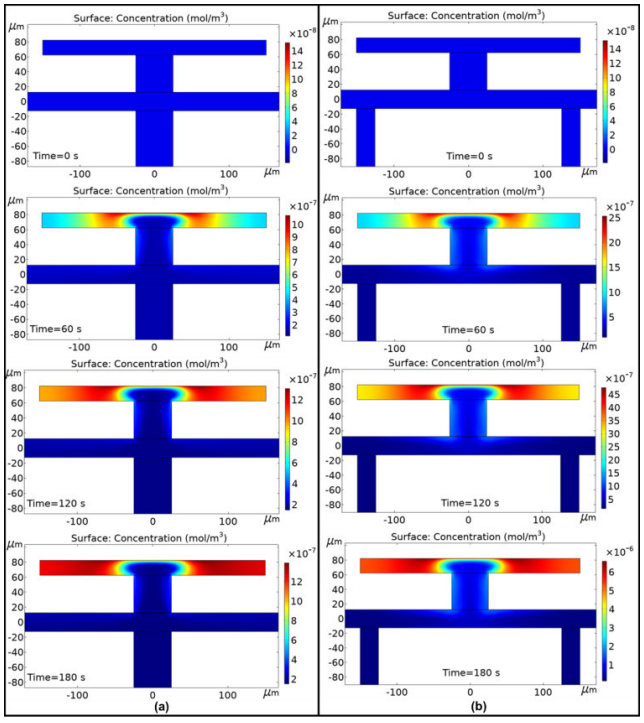

FIGURE 6. The examples of concentration process of DNA molecules as a function of time for the two improved configurations. (a) The improved configuration without the branch microchannels. (b) The improved configuration with the branch microchannels.

sample molecules. The eight diagrams show the concentration process with the time. Firstly, the sample molecules migrate from the Inlet to the electrode O region. Then, the sample molecules are accumulated near the region of electrode O gradually, as indicated by the increasing area of concentration and the change in color scale from the initial blue color to red finally. It should be noted that the solution with the DNA molecules continuously flows into the enrichment chamber. Hence the blue color presents in the center of the enrichment chamber all the time. According to the flow field in the enrichment chamber, the velocity of the sample solution reduces greatly from the center region of the electrode O to the both ends. Therefore, with the time goes by, the DNA molecules diffuse to the both ends from the center to form the concentration region.

TABLE 2. The comparison of enrichment rate between the two configurations.

Time (s)	0	30	60	90	120	150	180
$c_1(t)/c_0$	0	1.67	3.72	4.92	5.87	6.38	6.76
$c_2(t)/c_0$	0	2.29	8.29	14.4	20.3	25.7	30.6

The enrichment process of the two improved microchannel configurations is similar, however, the enrichment rate (defined as the ratio between the average concentration of the enrichment chamber and the initial concentration of the Inlet) is obviously different. In order to determine the efficiency of the concentration process, the average concentration of the sample molecules was calculated for the enrichment chamber at different times. Table 2 shows a comparison of the enrichment efficiency between two improved configurations within 180s under the same conditions. In Table 2, $c_1(t)$ and $c_2(t)$ represent the average concentration of DNA molecules in the enrichment chamber for the two improved configurations, respectively. c_0 denotes the initial concentration of DNA molecules. It can be seen that the enrichment rate of the configuration with branch microchannels is about 4.5-fold higher than that of the configuration without branch microchannels at $t = 180$ s.

B. EFFECTS OF VARIO◦ 76US PARAMETERS

Since the enrichment efficiency of the configuration with branch microchannels is much better, a further investigation of optimal parameters was carried out on this configuration, including the dimensions of the transition chamber, the enrichment chamber, and the branch microchannels, as well as the electric field intensity.

1) THE SIZE EFFECT OF THE TRANSITION CHAMBER

As we mentioned above, the transition chamber is the 'first gate' to control the flow of the sample solution. Therefore, the size of transition chamber may affect the enrichment efficiency significantly. Fig. 7 shows the effect of the width (W_3) and length (L_3) of the transition chamber on the concentration process. For better comparison, all parameters used in Fig. 5 were kept fixed except for the size of transition chamber. In this case, the voltages at electrode O, A and B were set to 0 V, 40V and 40V, respectively. As shown in Fig. 7 (a), the enrichment rate is inversely proportional to the width of the transition chamber. Fig. 7 (b) shows that the enrichment rate increases as the length of transition chamber. Since reducing the width or increasing the length of the transition may increase the fluid resistance, it has a big impact on the outflow of the sample solution. These two cases show that a narrower and longer transition chamber has the better enrichment efficiency within the same time period.

2) THE SIZE EFFECT OF THE ENRICHMENT CHAMBER

Figures that are composed of only black lines and shapes. These figures should have no shades or half-tones of gray, only black and white.

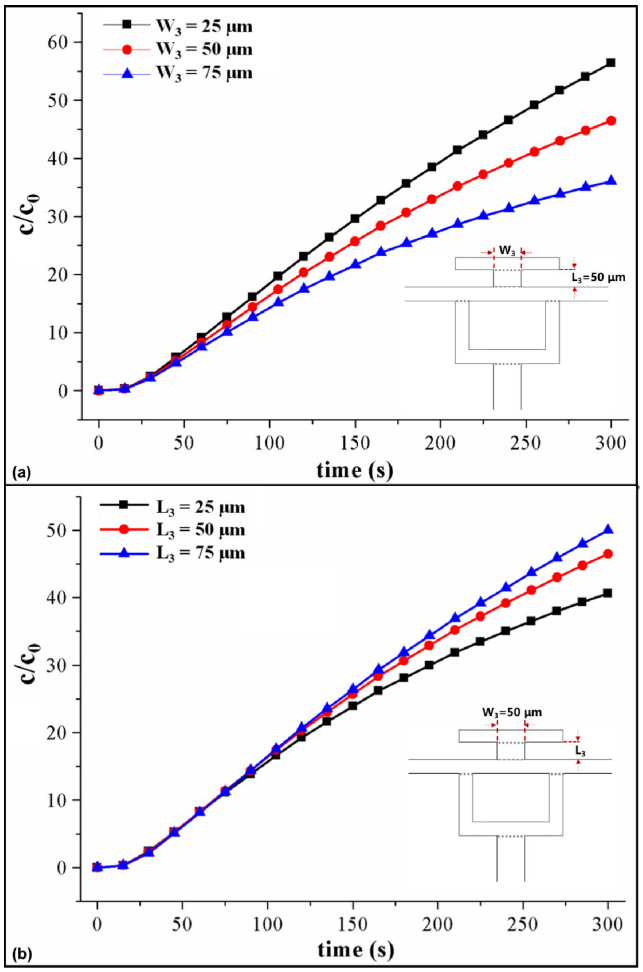

FIGURE 7. The size effect of the transition chamber for concentrating DNA molecules. (a) Curves of the enrichment rate over time by changing the width. (b) Curves of the enrichment rate over time by changing the length.

The enrichment efficiency is directly affected by the change of the size of the enrichment chamber. Theoretically, the larger the enrichment chamber is, the lower the average concentration will be under the same condition. In other words, the larger the enrichment chamber is, the longer time will be required to obtain the same enrichment rate. For comparison, all parameters used in Fig. 5 were fixed except for the size of enrichment chamber. In this case, the voltages at electrode O, A and B were set to 0 V, 40V and 40V, respectively. The size effect of the enrichment chamber on the concentration process is plotted in Fig. 8. As can be seen in Fig. 8 (a), increasing the length of the enrichment chamber may decrease the enrichment rate. However, when the time is long enough, *i. e.* 1200 s, the enrichment rate tends to be closed of different length of the enrichment chamber. Fig. 8 (b) shows the enrichment rate of the different width of the enrichment chamber over time. It is seen that the enrichment rate is inversely proportional to the width of the enrichment chamber. If the width of the enrichment chamber decreases, the enrichment rate increases greatly. The reduction of the area of the enrichment chamber enhances the

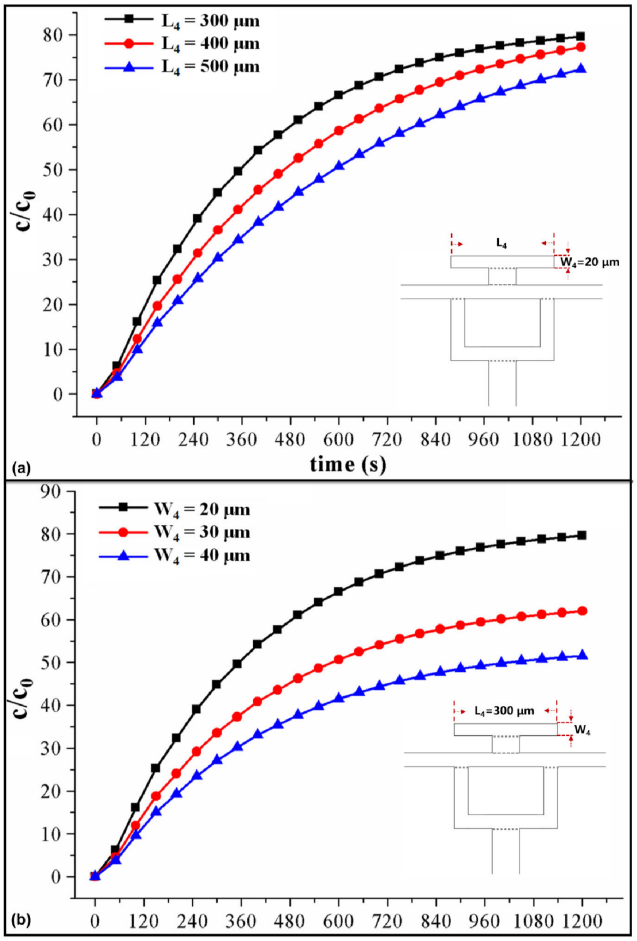

FIGURE 8. The size effect of enrichment chamber for concentrating DNA molecules. (a) Curves of the enrichment rate over time by changing the width. (b) Curves of the enrichment rate over time by changing the length.

adsorption ability to DNA molecules by electrostatic force, therefore, a small size of the enrichment chamber can reach the given concentration faster in the same time period.

3) EFFECT OF THE LENGTH OF THE BRANCH CHANNELS

The main difference between the two improved configurations is the branch channels. As mentioned above, the branch channels is the 'second gate' to control the flow of the sample solution. The branch channels may significantly affect the outflow of the sample solution by increasing the resistance of fluid and weakening the drag force of electroosmosis, resulting in enhancing the enrichment efficiency. In this simulation, we mainly studied the influence of the length of the horizontal branch for the concentration process. All parameters used in Fig. 5 were fixed except for the size of branch channels. In this case, the voltages at electrode O, A and B were set to 0 V, 40V and 40V, respectively. The relationship between the enrichment rate and time under different lengths are shown in Fig. 9. It is seen that the enrichment rate increases with the increase of the length of the horizontal branch. Obviously, the increase of the length of the horizontal branch helps to

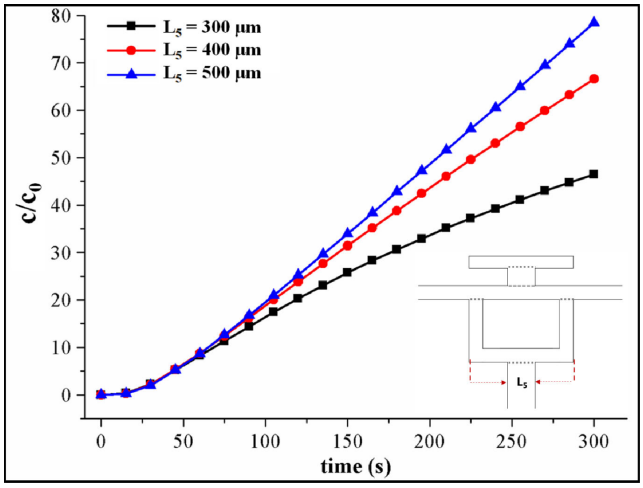

FIGURE 9. The size effect of branch channels for concentrating DNA molecules. Curves of the enrichment rate over time by changing the length.

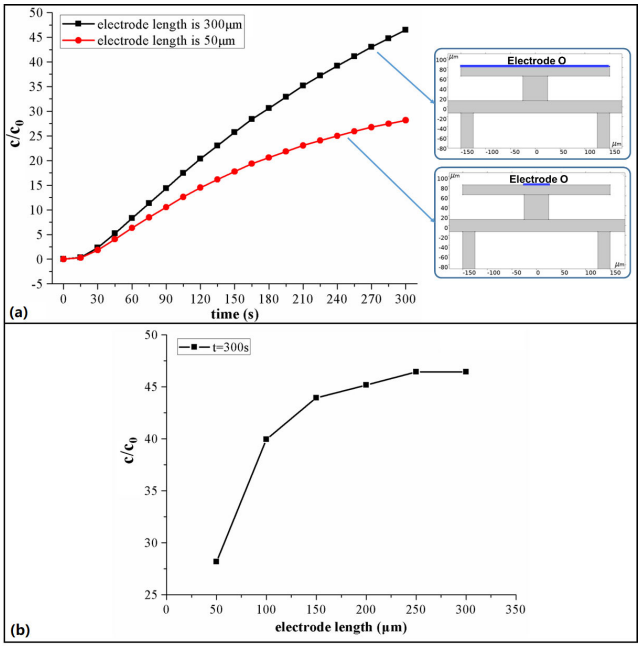

FIGURE 10. The size effect of electrode for concentrating DNA molecules. (a) Curves of the enrichment rate over time by changing the length of the electrode. (b) Curve of the enrichment rate for the different length of electrode O at t = 300 s.

increase the enrichment rate. The reason for this is that the longer length of the horizontal branch enhances the resistance of fluid. However, this is not a linear relationship.

4) EFFECT OF THE ELECTRODE SIZE

The influence of the electrode size on the enrichment rate was studied by changing the length of the electrode O, as shown in Fig. 10. In this simulation, all parameters used in Fig. 5 were fixed. The voltages at electrode O, A and B were set to 0 V, 40V and 40V, respectively. As shown in Fig. 10 (a), the longer electrode can adsorb more DNA molecules and hence the enrichment rate increases. As seen

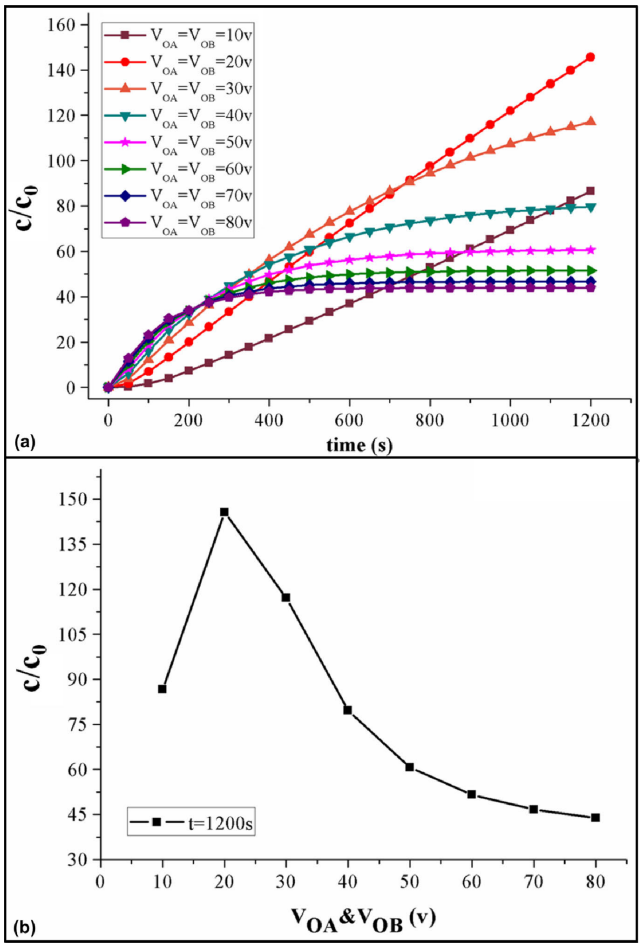

FIGURE 11. (a) Curves of the enrichment rate over time by changing the electric field intensity. (b) The relationship between the enrichment rate and applied voltages at t = 1200 s.

clearly in Fig. 10 (b), the dependence of the concentration rate is not a linear function of the electrode size. Once the length of electrode is longer than 250 μm, the concentration rate becomes constant. In the 2D model, electrode O forms the wall of the enrichment chamber. According to the previous analysis shown in Fig. 5, the current density and flow velocity decrease from the middle region of the enrichment chamber to both ends rapidly. Therefore, when the length of electrode O reaches a certain value, its effect on enrichment rate becomes very weak.

5) EFFECT OF ELECTRIC FIELD INTENSITY

The applied electric field has at least two effects on the concentration process. It drives the negatively charged sample molecules to move to the enrichment chamber and creates the electrostatic force to adsorb the negatively charged sample molecules. The change of the electric field intensity will undoubtedly affect the enrichment effect. In this simulation, all parameters used in Fig. 5 were fixed. The voltages at electrode O, A and B were set to 0 V, V_{OA} and V_{OB}, respectively.

The effect of the electrical field on the concentration process is plotted in Fig. 11 (a). At the beginning (shown in blue dash line), the enrichment rate increases with the increase of the electrical field intensity for the same concentration time. However, after about 215 s, the enrichment rate gradually becomes equilibrium over time. If the applied voltage is large, i.e. 40 V $\sim$ 80 V, the enrichment rate is not a linear function of the electrical field intensity. The large applied voltage can generate strong electroosmotic flow, which can quickly bring out the sample molecules from the enrichment chamber. Over time, the inflow and outflow of the sample molecules will achieve a balance point and the enrichment rate will not increase anymore. Therefore, the large applied voltage may fail to generate the good enrichment effect. Fig. 11 (b) shows that when the applied voltage is 20 V, the enrichment rate can reach 145.7 at t = 1200 s. However, when the applied voltage is 80 V, the enrichment rate is only about 45 at t = 1200 s.

V. CONCLUSION

A T-shaped microfluidic chip model for the enrichment of DNA molecules was established and numerically analyzed. A variety of factors such as the dimensions of the transition chamber, the enrichment chamber, and the branch microchannels, as well as the electric field intensity were investigated to evaluate their influence on the enrichment effect. The simulation results show that high concentration of DNA molecules was obtained by the optimal configuration of the microfluidic channels and the electric field intensity. For instance, when taking the microchannel sizes of 25 μm (W_3), 75 μm (L_3), 20 μm (W_4), 300 μm (L_4), 200 μm (W_5), of 500 μm (L_5), and the length of electrode O of 300 μm, an enrichment rate of 234.2 at t = 1200s can be obtained when the applied voltage is 20 V. The numerical analysis of the developed T-shaped microfluidic model provides a good guidance for the design of the microfluidic enrichment chip. The proposed method does not require any complex structure and AC field and may lead to develop a simple and practical microfluidic chip for sample concentration in dilute solutions.

REFERENCES

[1] T. N. T. Dao, J. Yoon, C. E. Jin, B. Koo, K. Han, Y. Shin, and T. Y. Lee, "Rapid and sensitive detection of Salmonella based on microfluidic enrichment with a label-free nanobiosensing platform," *Sens. Actuators B, Chem.*, vol. 262, pp. 588–594, Jun. 2018.
[2] Y. Li, X. Yan, X. Feng, J. Wang, W. Du, Y. Wang, P. Chen, L. Xiong, and B.-F. Liu, "Agarose–based microfluidic device for point-of-care concentration and detection of pathogen," *Anal. Chem.*, vol. 86, no. 21, pp. 10653–10659, Nov. 2014.
[3] X. Weng, W. Zhao, S. Neethirajan, and T. Duffield, "Microfluidic biosensor for Hydroxybutyrate (HBA) determination of subclinical ketosis diagnosis," *J. Nanobiotechnol.*, vol. 13, no. 1, p. 13, 2015.
[4] D. Gao, H. Liu, Y. Jiang, J.-M. Lin, D. Gao, H. Liu, and Y. Jiang, "Recent developments in microfluidic devices for *in vitro* cell culture for cell-biology research," *TrAC Trends Anal. Chem.*, vol. 35, pp. 150–164, May 2012.
[5] S. Sarkar, P. Sabhachandani, D. Stroopinsky, K. Palmer, N. Cohen, J. Rosenblatt, D. Avigan, and T. Konry, "Dynamic analysis of immune and cancer cell interactions at single cell level in microfluidic droplets," *Biomicrofluidics*, vol. 10, no. 5, Sep. 2016, Art. no. 054115.
[6] X. Weng and S. Neethirajan, "Ensuring food safety: Quality monitoring using microfluidics," *Trends Food Sci. & Technol.*, vol. 65, pp. 10–22, Jul. 2017.
[7] X. Weng and S. Neethirajan, "A microfluidic biosensor using graphene oxide and aptamer-functionalized quantum dots for peanut allergen detection," *Biosens. Bioelectron.*, vol. 85, pp. 649–656, Nov. 2016.

[8] L. Marle and G. M. Greenway, "Microfluidic devices for environmental monitoring," *TRAC Trends Anal. Chem.*, vol. 24, no. 9, pp. 795–802, Oct. 2005.

[9] C. S. Luke, J. Selimkhanov, L. Baumgart, S. E. Cohen, S. S. Golden, N. A. Cookson, and J. Hasty, "A microfluidic platform for long–term monitoring of algae in a dynamic environment," *ACS Synth. Biol.*, vol. 5, no. 1, pp. 8–14, Jan. 2016.

[10] X. Weng, Y. Kang, Q. Guo, B. Peng, and H. Jiang, "Recent advances in thread-based microfluidics for diagnostic applications," *Biosens. Bioelectron.*, vol. 132, pp. 171–185, May 2019.

[11] H. Jiang, X. Weng, and D. Q. Li, "Dual-wavelength fluorescent detection of particles on a novel microfluidic chip," *Lab Chip*, vol. 13, no. 5, pp. 843–850, 2013.

[12] X. Weng, S. R. Ahmed, and S. Neethirajan, "A nanocomposite-based biosensor for bovine haptoglobin on a 3D paper-based analytical device," *Sens. Actuators B, Chem.*, vol. 265, pp. 242–248, Jul. 2018.

[13] C.-C. Lin, J.-L. Hsu, and G.-B. Lee, "Sample preconcentration in microfluidic devices," *Microfluid Nanofluid*, vol. 10, no. 3, pp. 481–511, Mar. 2011.

[14] C. Zhao, Z. Ge, and C. Yang, "Microfluidic techniques for analytes concentration," *Micromachines*, vol. 8, no. 1, p. 28, Jan. 2017.

[15] L.-M. Fu, H.-H. Hou, P.-H. Chiu, and R.-J. Yang, "Sample preconcentration from dilute solutions on micro/nanofluidic platforms: A review," *Electrophoresis*, vol. 39, no. 2, pp. 289–310, Jan. 2018.

[16] J. P. Quirino and S. Terabe, "Sweeping of analyte zones in electrokinetic chromatography," *Anal. Chem.*, vol. 71, no. 8, pp. 1638–1644, Apr. 1999.

[17] J. P. Quirino, J.-B. Kim, and S. Terabe, "Sweeping: Concentration mechanism and applications to high-sensitivity analysis in capillary electrophoresis," *J. Chromatography A*, vol. 965, nos. 1–2, pp. 357–373, Aug. 2002.

[18] A. T. Aranas, A. M. Guidote, and J. P. Quirino, "Sweeping and new online sample preconcentration techniques in capillary electrophoresis," *Anal Bioanal Chem*, vol. 394, no. 1, pp. 175–185, May 2009.

[19] A. Wuethrich, P. R. Haddad, and J. P. Quirino, "Electrophoretic concentration and sweeping-micellar electrokinetic chromatography analysis of cationic drugs in water samples," *J. Chromatography A*, vol. 1401, pp. 84–88, Jul. 2015.

[20] C.-X. Zhang and W. Thormann, "Head–column field–amplified sample stacking in binary system capillary electrophoresis: A robust approach providing over 1000-fold sensitivity enhancement," *Anal. Chem.*, vol. 68, no. 15, pp. 2523–2532, Jan. 1996.

[21] B. Jung, R. Bharadwaj, and J. G. Santiago, "Thousandfold signal increase using field-amplified sample stacking for on-chip electrophoresis," *Electrophoresis*, vol. 24, no. 1920, pp. 3476–3483, Oct. 2003.

[22] S. Dziomba, P. Kowalski, and T. Bączek, "Field-amplified sample stacking–sweeping of vitamins B determination in capillary electrophoresis," *J. Chromatography A*, vol. 1267, pp. 224–230, Dec. 2012.

[23] L. Liu, Q. Wan, X. Xu, S. Duan, and C. Yang, "Combination of micelle collapse and field-amplified sample stacking in capillary electrophoresis for determination of trimethoprim and sulfamethoxazole in animal-originated foodstuffs," *Food Chem.*, vol. 219, pp. 7–12, Mar. 2017.

[24] B. Ma, X. Zhou, G. Wang, H. Huang, Z. Dai, J. Qin, and B. Lin, "Integrated isotachophoretic preconcentration with zone electrophoresis separation on a quartz microchip for UV detection of flavonoids," *Electrophoresis*, vol. 27, no. 24, pp. 4904–4909, Dec. 2006.

[25] B. Jung, R. Bharadwaj, and J. G. Santiago, "On–chip millionfold sample stacking using transient isotachophoresis," *Anal. Chem.*, vol. 78, no. 7, pp. 2319–2327, Apr. 2006.

[26] D. Bottenus, M. R. Hossan, Y. Ouyang, W.-J. Dong, P. Dutta, and C. F. Ivory, "Preconcentration and detection of the phosphorylated forms of cardiac troponin I in a cascade microchip by cationic isotachophoresis," *Lab Chip*, vol. 11, no. 22, pp. 3793–3801, 2011.

[27] B. Y. Moghadam, K. T. Connelly, and J. D. Posner, "Two orders of magnitude improvement in detection limit of lateral flow assays using isotachophoresis," *Anal. Chem.*, vol. 87, no. 2, pp. 1009–1017, Jan. 2015.

[28] P. G. Righetti and A. Bossi, "Isoelectric focusing of proteins and peptides in gel slabs and in capillaries," *Analytica Chim. Acta*, vol. 372, nos. 1–2, pp. 1–19, 1998.

[29] R. Montgomery, X. Jia, and L. Tolley, "Dynamic isoelectric focusing for proteomics," *Anal. Chem.*, vol. 78, no. 18, pp. 6511–6518, Sep. 2006.

[30] J. Shim, P. Dutta, and C. F. Ivory, "Effects of ampholyte concentration on protein behavior in on-chip isoelectric focusing," *Electrophoresis*, vol. 29, no. 5, pp. 1026–1035, Mar. 2008.

[31] W. S. Koegler and C. F. Ivory, "Focusing proteins in an electric field gradient," *J. Chromatography A*, vol. 726, nos. 1–2, pp. 229–236, Mar. 1996.

[32] D. N. Petsev, G. P. Lopez, C. F. Ivory, and S. S. Sibbett, "Microchannel protein separation by electric field gradient focusing," *Lab Chip*, vol. 5, no. 6, p. 587, 2005.

[33] C. A. Trickett, R. D. Henderson, R. M. Guijt, and M. C. Breadmore, "Electric field gradient focusing using a variable width polyaniline electrode," *Electrophoresis*, vol. 33, no. 21, pp. 3254–3258, Nov. 2012.

[34] K. M. Balss, W. N. Vreeland, K. W. Phinney, and D. Ross, "Simultaneous concentration and separation of enantiomers with chiral temperature gradient focusing," *Anal. Chem.*, vol. 76, no. 24, pp. 7243–7249, Dec. 2004.

[35] M. S. Munson, J. M. Meacham, D. Ross, and L. E. Locascio, "Development of aptamer-based affinity assays using temperature gradient focusing: Minimization of the limit of detection," *Electrophoresis*, vol. 29, no. 16, pp. 3456–3465, Aug. 2008.

[36] Z. Ge, W. Wang, and C. Yang, "Towards high concentration enhancement of microfluidic temperature gradient focusing of sample solutes using combined AC and DC field induced Joule heating," *Lab Chip*, vol. 11, no. 7, pp. 1396–1402, 2011.

[37] Z. Ge, W. Wang, and C. Yang, "Rapid concentration of deoxyribonucleic acid via Joule heating induced temperature gradient focusing in polydimethylsiloxane microfluidic channel," *Analytica Chim. Acta*, vol. 858, pp. 91–97, Feb. 2015.

[38] J. Dai, T. Ito, L. Sun, and R. M. Crooks, "Electrokinetic trapping and concentration enrichment of DNA in a microfluidic channel," *J. Amer. Chem. Soc.*, vol. 125, no. 43, pp. 13026–13027, Oct. 2003.

[39] S. H. Ko, Y.-A. Song, S. J. Kim, M. Kim, J. Han, and K. H. Kang, "Nanofluidic preconcentration device in a straight microchannel using ion concentration polarization," *Lab Chip*, vol. 12, no. 21, pp. 4472–4482, 2012.

[40] R.-J. Yang, H.-H. Pu, and H.-L. Wang, "Ion concentration polarization on paper-based microfluidic devices and its application to preconcentrate dilute sample solutions," *Biomicrofluidics*, vol. 9, no. 1, Jan. 2015, Art. no. 014122.

[41] D.-T. Phan, S. A. M. Shaegh, C. Yang, and N.-T. Nguyen, "Sample concentration in a microfluidic paper- based analytical device using ion concentration polarization," *Sens. Actuators B, Chem.*, vol. 222, pp. 735–740, Jan. 2016.

[42] L. Yang, P. P. Banada, M. R. Chatni, K. Seop Lim, A. K. Bhunia, M. Ladisch, and R. Bashir, "A multifunctional micro-fluidic system for dielectrophoretic concentration coupled with immuno-capture of low numbers of Listeria monocytogenes," *Lab Chip*, vol. 6, no. 7, pp. 896–905, 2006.

[43] N. Gadish and J. Voldman, "High–throughput positive–dielectrophoretic bioparticle microconcentrator," *Anal. Chem.*, vol. 78, no. 22, pp. 7870–7876, Nov. 2006.

[44] A. Sharma, C.-H. Han, and J. Jang, "Rapid electrical immunoassay of the cardiac biomarker troponin I through dielectrophoretic concentration using imbedded electrodes," *Biosens. Bioelectron.*, vol. 82, pp. 78–84, Aug. 2016.

[45] J. P. Gleghorn, E. D. Pratt, D. Denning, H. Liu, N. H. Bander, S. T. Tagawa, D. M. Nanus, P. A. Giannakakou, and B. J. Kirby, "Capture of circulating tumor cells from whole blood of prostate cancer patients using geometrically enhanced differential immunocapture (GEDI) and a prostate-specific antibody," *Lab Chip*, vol. 10, no. 1, pp. 27–29, Nov. 2009.

[46] F. I. Thege, T. B. Lannin, T. N. Saha, S. Tsai, M. L. Kochman, M. A. Hollingsworth, A. D. Rhim, and B. J. Kirby, "Microfluidic immunocapture of circulating pancreatic cells using parallel EpCAM and MUC1 capture: Characterization, optimization and downstream analysis," *Lab Chip*, vol. 14, no. 10, pp. 1775–1784, Feb. 2014.

[47] J. J. Yoo, M. J. Anderson, T. M. Alligrant, and R. M. Crooks, "Electrochemical detection of insulating beads at subattomolar concentration via magnetic enrichment in a microfluidic device," *Anal. Chem.*, vol. 86, no. 9, pp. 4302–4307, May 2014.

[48] L.-L. Fan, X.-L. Zhu, Q. Yan, J. Zhe, and L. Zhao, "A passive microfluidic device for continuous microparticle enrichment," *Electrophoresis*, vol. 40, no. 6, pp. 1000–1009, Mar. 2019.

[49] D. Zhao, Z. He, G. Wang, H. Wang, Q. Zhang, and Y. Li, "Three-dimensional ordered titanium dioxide-zirconium dioxide film-based microfluidic device for efficient on-chip phosphopeptide enrichment," *J. Colloid Interface Sci.*, vol. 478, pp. 227–235, Sep. 2016.

[50] M. Jia and T. Kim, "Multiphysics Simulation of ion concentration polarization induced by nanoporous membranes in dual channel devices," *Anal. Chem.*, vol. 86, no. 15, pp. 7360–7367, Aug. 2014.

[51] L. Gong, W. Ouyang, Z. Li, and J. Han, "Direct numerical simulation of continuous lithium extraction from high Mg2+/Li+ ratio brines using microfluidic channels with ion concentration polarization," *J. Membrane Sci.*, vol. 556, pp. 34–41, Jun. 2018.
[52] Y. Daghighi and D. Li, "Numerical studies of electrokinetic control of DNA concentration in a closed-end microchannel," *Electrophoresis*, vol. 31, no. 5, pp. 868–878, Mar. 2010.
[53] H. Jiang, Y. Daghighi, C. H. Chon, and D. Li, "Concentrating molecules in a simple microchannel," *J. Colloid Interface Sci.*, vol. 347, no. 2, pp. 324–331, Jul. 2010.
[54] H. Jiang, N. Fan, B. Peng, and X. Weng, "Characterization of an induced pressure pumping force for microfluidics," *Appl. Phys. Lett.*, vol. 110, no. 18, May 2017, Art. no. 184102.
[55] N. A. Patankar and H. H. Hu, "Numerical simulation of electroosmotic flow," *Anal. Chem.*, vol. 70, no. 9, pp. 1870–1881, May 1998.

YANLI GONG received the B.Eng. degree in communication engineering from Shandong Technology and Business University, in 2009, and the M.Eng. degree in optical engineering from the University of Electronic Science and Technology of China (UESTC), Chengdu, China, in 2012, where she is currently pursuing the Ph.D. degree in mechanical engineering. Her research interests mainly include microfluidic enrichment and detection technology and its application.

HAI JIANG received the B.Sc. and M.Sc. degrees in biomedical engineering from Chongqing University, in 2003 and 2007, respectively, and the Ph.D. degree in mechanical engineering from the University of Waterloo, in 2014. He worked with the University of British Columbia, as a postdoctoral position, from 2014 to 2015. He is currently an Associate Professor with the School of Mechanical and Electrical Engineering, University of Electronic Science and Technology of China. He has published more than 20 academic articles in high-impact international academic journals. He has a high-level output of research publications in leading international journals and presentations at international conferences in the research areas of microfluidics and its applications, which demonstrates significant research and grant potential in engineering and cross-disciplinary applications.

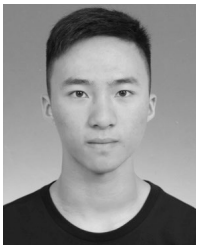

YUNFEI BAI was born in 1999. He is currently pursuing the bachelor's degree in mechanical engineering with the University of Electronic Science and Technology of China. He participated with the college students' Innovation and Entrepreneurship Project, from 2018 to 2019, which named "study on sample concentration detection method based on microfluidic technology".

ZIJIAN WU was born in 1997. He is currently pursuing the bachelor's degree in mechanical engineering with the University of Electronic Science and Technology of China. He participated with the college students' Innovation and Entrepreneurship Project, from 2018 to 2019, which named "study on glucose concentration detection method based on microfluidic technology".

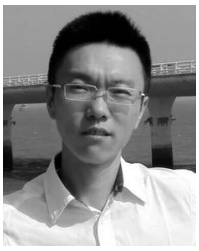

BEI PENG received the B.S. degree from Beihang University, in 2009, and the M.S. and Ph.D. degrees from Northwestern University, in 2003 and 2008, respectively. He is currently a Full Professor of mechatronics engineering with the University of Electronic Science and Technology of China. He holds 30 authorized patents. He has served as a PI or a Co-PI for over ten research projects, including the National Science Foundation of China (NSFC). He has published over 100 journal articles and conference papers. His research interests mainly include intelligent manufacturing systems, nano material design, and its applications.

XUAN WENG received the B.Sc. and M.Sc. degrees major in biomedical engineering from Chongqing University, China, in 2003 and 2007, respectively, and the Ph.D. degree in mechanical engineering from the University of Waterloo, Canada. She worked with the University of Guelph, as a Postdoctoral Fellow, from 2014 to 2018. She is currently a Professor with the School of Mechanical and Electrical Engineering, University of Electronic Science and Technology of China. By virtue of her expertise, she has published more than 30 scientific articles in various high impact international journals. She made great achievement in the multidisciplinary research field of microfluidics, biosensor, and nanotechnology.